Chapter 1

Simulating structure and physical properties of complex metallic alloys

Hans-Rainer Trebin, Peter Brommer, Michael Engel, Franz Gähler,
Stephen Hocker, Frohmut Rösch and Johannes Roth

Institut für Theoretische und Angewandte Physik, Universität Stuttgart

An introduction is presented to numerical methods, by which the behavior of complex metallic alloys can be simulated. We primarily consider the molecular dynamics (MD) technique as implemented in our software package IMD, where Newton's equations of motion are solved for all atoms in a solid. After a short discourse on integration algorithms, some possible types of interactions are addressed. Already simple model potentials, as for example the Lennard-Jones-Gauss potential, can give rise to complex structures, where the characteristic length scales of the order by far exceed the range of the pair interaction. Realistic interactions are modelled by highly parametrized effective potentials, like the EAM (Embedded Atom Method) potential. Our program potfit allows to fit the parameters such that data from experiment or from ab-initio calculations are well reproduced. Several applications of the methods are outlined, notably the simulation of aluminium diffusion in quasicrystalline d-Al-Ni-Co, the computation of the phonon dispersion via the dynamical structure factor of $MgZn_2$, the propagation of cracks in $NbCr_2$, and an order-disorder phase transition in $CaCd_6$.

1.1. Numerical simulation of matter

The basic equation for computing the structure of atomistic matter is known since the invention of quantum theory: It is the many-body Schrödinger equation. Powerful analytical tools have been developed in the sequel to make it solvable. For periodic crystals, the Bloch theorem and the Kohn-Sham density functional theory allowed to determine ground state structures, cohesion energies and electronic band structures. Within the Born-Oppenheimer approximation, phonon dispersion relations, dynamical and even and non-equilibrium properties can be evaluated.

2 *H.-R. Trebin et al.*

Explicit realistic data were gained, however, only with the advent of computers and efficient algorithms. Yet, when dealing with complex metallic alloys, where the number of atoms in the unit cell is large, and when exploring phenomena, where periodic boundary conditions are hardly applicable, like defect motion or fracture, the power of even massively parallel computer systems is not suffient. The same is valid when long simulation times are required, as for example for diffusion processes. For such cases one employs an approximation denoted molecular dynamics (MD). The atoms are considered as point particles of classical mechanics, which move according to Newton's equations of motion under their mutual (but possibly also external) forces. The atom-atom interactions are the central quantities that tune the resulting physical properties. In principle, these interaction could even be computed quantum-mechanically, e.g. in density functional theory under the Born-Oppenheimer approximation, where it is assumed that the electronic degrees of freedom are always in the instantaneous ground state for a given set of nuclear coordinates. For large systems, however, this is far too slow, and it is more promising to use a classical effective potential approximating the quantum-mechanical interaction. As classical potentials are much cheaper to compute, far larger systems and longer time scales can be reached in this way.

Many efforts have been made to understand the response of the particle systems to different types of interaction potentials. A simple isotropic pair potential like the Lennard-Jones potential with a single minimum typically yields densely packed simple structures as found in many hexagonal or face centered cubic monoatomic metals. Even with such simple potentials, it is possible to explain e.g. the formation and motion of partical dislocations. With binary systems or modified potentials, e.g. with an additional bump or minimum, more complicated structures may be reached, whose period lengths can by far exceed the range of the potential and which we hence denote as *complex*. For realistic simulations of particular materials, however, it is necessary to go beyond such model potentials. For various types of materials there exist highly parametrized potential models taylored for the specific situation, e.g. for metallic, covalent, or ionic systems. The parameters are fitted such that either experimental data (melting temperature, elastic constants, cohesion energies) or data from quantum mechanical calculations of small systems (cohesion energies, stresses, forces on individual atoms) are optimally reproduced. With such realistic potentials and efficient algorithms on supercomputers it is possible to routinely simulate even the most demanding situations with high reliability, whether they require

Simulation of complex metallic alloys   3

large system sizes (crack propagation, shock waves, dislocation entanglement) with up to several hundred million atoms, or long simulation times (atomic diffusion). But also equilibrium material parameters (elastic constants, heat conductivities, toughness) can be extracted and used as input for continuum theories. By forwarding data from quantum mechanical ab-initio calculations to molecular dynamics simulations and further to continuum theories (e.g. finite element methods) one can establish a multi-scale algorithm by which matter can be analysed up to mesoscopic length scales.

A problem remaining is the span of real time achieveable in MD simulations, which reaches up to the order of nanoseconds, but not much beyond. Stochastic methods like the Monte Carlo algorithm may then be used to accelerate equilibration processes, where it is not necessary to track precisely the physical trajectories of the particles. Rather, the displacements of the atoms are chosen probabilistically, with weights depending on the energy gain achieved. By eliminating irrelevant degrees of freedom from the set of proposed moves, a considerable speed-up can be achieved, compared to MD. There are many other accelerators on the market like dissipative particle dynamics (PDP) or stochastic rotation dynamics (SRD), which average out short-time motions, but we will not dwell upon them further.

In this article we will proceed as follows. In Sec. 1.2 the molecular dynamics method is described. In particular, we sketch some popular integration methods and show how modified equations of motion can be used to simulate different kinds thermodynamic ensembles, e.g. ones which allow to control temperature, pressure, or shear. In Sec. 1.3 several model potentials are introduced, and some of the possible complex structures they generate are described. In Sec. 1.4 we show examples of realistic potentials, and discuss their range of validity. In Sec. 1.5 it is then demonstrated how the optimal potential paramters can be determined from results of ab-initio simulations, thus making quantum-mechanical information available also to classical simulations. Several potentials of embedded-atom-method (EAM) type have been generated by this method and were used in simulations of various physical properties and processes, such as atomic diffusion, phonon dispersion, crack propagation and a phase transition. These applications are described in Sec. 1.6, before we summarize in Sec. 1.7.

1.2. Molecular dynamics simulations

In molecular dynamics (MD) simulations[1–3] the trajectories of particles in a many-body system are calculated in classical approximation. Thus

4   *H.-R. Trebin et al.*

Newton's equations

$$\frac{dp_i}{dt} = F_i = -\nabla_i V(r_1, \ldots, r_N), \tag{1.1}$$

$$\frac{dr_i}{dt} = \frac{p_i}{m_i}, \tag{1.2}$$

have to be solved under a specific interaction potential V. Here $r_1, \ldots, r_N$ are the coordinate vectors of the particles and $p_1, \ldots, p_N$ their momenta.

In a first step one must establish an initial structure in the form of particle coordinates for the different atomic species. This can be done by either distributing the particles randomly, or using a model structure or a realistic structure derived from experimental (e.g. diffraction) data.

In a second step the interaction potentials have to be determined. These can be two-, three- or many-body potentials. They can be model potentials, addressed in Sec. 1.3, as for example the Lennard-Jones pair potential and modifications thereof. Or one chooses realistic effective potentials, fitted to experimental or ab-initio data, as discussed in Sec. 1.4 and 1.5.

In a third step the boundary conditions must be fixed. One can apply open bounderies or enclose the system in a hard box. In most instances periodic boundary conditions are chosen. They allow to simulate an infinite system by packing it into a periodically repeated array of unit cells. Thus one can avoid the influence of surfaces. But even for the calculation of surfaces frequently periodic boundary conditions are used by simulating a periodic layer structure. For specific situations a variety of other boundary conditions have been invented. In Lees-Edward boundary conditions, for example, the periodically stacked boxes are displaced relative to each other with constant velocity to mimic a shear deformation. Or twisted boundaries can model chiral structures, as e.g. cholesteric liquid crystals.

Newton's equations form a $3N$-dimensional coupled set of second order differential equation for the particle trajectories $r_i(t)$. In a fourth step they must be solved by numerical integrators subject to requirements like high precision, stability, time-reversal symmetry, energy and momentum conservation. The conditions are met by the relatively simple expressions of the Verlet and leap-frog algorithms.

In the Verlet algorithm the Taylor expansions of $r_i(t + \delta t)$ and $r_i(t - \delta t)$,

$$r_i(t + \delta t) = r_i(t) + \delta t \dot{r}_i(t) + \frac{1}{2}(\delta t)^2 \ddot{r}_i(t) + \ldots, \tag{1.3}$$

$$r_i(t - \delta t) = r_i(t) - \delta t \dot{r}_i(t) + \frac{1}{2}(\delta t)^2 \ddot{r}_i(t) - \ldots, \tag{1.4}$$

Simulation of complex metallic alloys   5

are added such that the odd powers of δt vanish and the velocities do not appear explicitely:

$$r_i(t + \delta t) = 2r_i(t) - r_i(t - \delta t) + (\delta t)^2 \ddot{r}_i(t) + \dots \qquad (1.5)$$

with

$$\ddot{r}_i(t) =: a_i(t) = -\frac{1}{m_i}\nabla_i V(r_1, \dots, r_N). \qquad (1.6)$$

The algorithm is correct to order $(\delta t)^4$ and time-reversible as it is centered.

For short time-steps the term of order $(\delta t)^2$ is small compared to the $O(1)$-terms which leads to numerical imprecision. A modification avoiding this deficiency is the half-step leap-frog algorithm:

$$r_i(t + \delta t) = r_i(t) + \delta t\, \dot{r}_i(t + \frac{1}{2}\delta t), \qquad (1.7)$$

$$\dot{r}_i(t + \frac{1}{2}\delta t) = \dot{r}_i(t - \frac{1}{2}\delta t) + \delta t\, a_i(t). \qquad (1.8)$$

Here, only terms of $O(\delta t)$ appear. Moreover, the second order equation (1.5) is replaced by a first order one, in which also the velocities have become independent degrees of freedom. Inserting (1.7) and (1.8) into the centering procedure (1.3)-(1.5) shows that the leap-frog scheme is algebraically equivalent to Verlet. With the leap-frog integrator we can simulate the microcanonical NVE ensemble, where particle number N, volume V and energy E are kept constant. For other ensembles, like the canonical NVT ensemble, or the NpT-ensemble one must apply numerical thermostats and barostats.

Temperature and pressure control can be achieved with suitable modifications of the equations of motion, (1.1) and (1.2). Specifically, for a thermostat a (positive or negative) friction term is added, and for a barostat the box and all coordinates are rescaled. For a thermostat and barostat of Nosé-Hoover type, the modified equations of motion then read as follows:

$$\dot{p}_i = F_i - (\eta + \xi)\, p_i, \qquad (1.9)$$

$$\dot{r}_i = \frac{p_i}{m_i} + \xi r_i, \qquad (1.10)$$

$$\dot{\eta} = \frac{1}{\tau_T^2}\frac{T - T_{ext}}{T_{ext}}, \qquad (1.11)$$

$$\dot{\xi} = \frac{1}{\tau_p^2}\frac{V(p - p_{ext})}{Nk_B T_{ext}}, \qquad (1.12)$$

$$\dot{h} = \xi h. \qquad (1.13)$$

6   H.-R. Trebin et al.

Here, η and ξ are two extra dynamical degrees of freedom. η is a friction parameter, and ξ the rate of rescaling of the coordinates and the matrix of the box vectors, h. The amount of friction and rescaling is determined by the deviation of the actual temperature and pressure from the desired values, T_{ext} and p_{ext}. The actual temperature and pressure are computed from the coordinates and momenta:

$$T = \frac{1}{3Nk_B} \sum_i \frac{|p_i|^2}{m_i}, \tag{1.14}$$

$$pV = \frac{1}{3} \left(\sum_i \frac{|p_i|^2}{m_i} + \frac{1}{2} \sum_{i,j} r_{ij} \cdot F_{ij} \right), \tag{1.15}$$

where $r_{ij} = r_i - r_j$ and F_{ij} is the force atom j exerts on atom i. The time evolution of η and ξ is governed by time constants τ_T and τ_p, which must be chosen suitably to ensure the best possible coupling of η and ξ to the other degrees of freedom. If only a thermostat is needed, ξ can be chosen identically zero (and thus $\tau_p = \infty$). By using tensor quantities for p, p_{ext}, and ξ, it is also possible to simulate an arbitrary external stress tensor, and with similar types of equations even a constant shear flow can be modelled.

In a fifth step the usually large amount of data must be analyzed. It is possible to extract global quantities like cohesion energies or melting temperatures or elastic constants. Also static and time dependent correlation functions can be calculated, like density-density or velocity-velocity correlations. From them structural characteristics can be gained like the pair correlation function or transport coefficients such as diffusion constants or viscosities. By Fourier transformation of the density-density correlation the diffraction images can be obtained.

But frequently the local situation is of interest. Here the primary tool is the visualization of the structure. The atoms can be plotted directly as spheres. Additionally they can be colored, e.g. according to their energy content. Thus places of enhanced energy are marked, which usually are close to defects like vacancies or interstitials or dislocations. Or they are colored according to their number of next neighbours to image surfaces, e.g. cracks. Observables like energy or temperature can be averaged over small spatial regions and then depict propagation of phonons. Animations of atomic dynamics give insight into mechanisms like energy transfer from elastic dilation into the crack tip where bonds are broken. Thus numerical simulations combined with visualization bring us back from the diagrammatic representation of physics to a way manifest to the visual senses.

All algorithms mentioned in this and the following sections are implemented in our own MD code IMD.[4] The results discussed in Sec. 1.6 have been obtained with IMD, which supports a large variety of integrators, potential models and other features, making it an excellent choice for the simulation of complex metals. Simple metals and even covalent solids are also supported, of course. IMD is efficiently parallelized and shows excellent performance and scaling on a large variety of hardware, from simple Linux PCs to massively parallel supercomputers.[5]

1.3. Model potentials

1.3.1. *Lennard-Jones potentials*

The Lennard-Jones potential (see Fig. 1.1)

$$v(r) = \epsilon((\frac{\sigma}{r})^{12} - 2(\frac{\sigma}{r})^6) \qquad (1.16)$$

is an interaction widely applied in statistical physics. It is particularly suited for noble gases. Frequently it has been used also for the simulation of metals as long as computing power was too small to treat more complicated interactions and better descriptions like EAM potentials had not been developed. The potential was invented by Sir John Edward Lennard-Jones (1894-1954) in 1924 for quantum chemistry applications. The mathematical form was chosen such that it is possible to evaluate integrals easily.

The stable solid phase of the Lennard-Jones potential in two dimensions is the hexagonal close packing. Thermodynamical properties and the phase diagram have been given by Abraham.[6]

In three dimensions the energetic ground state is the hexagonal close packing (hcp) which is slightly more stable than fcc.[7] Reference 7 also includes many citations of Lennard-Jones system properties like virial coefficients and thermodynamic and transport properties.

The thermodynamic phase diagram has been determined to high precision.[2,8,9]

In statistical physics the Lennard-Jones potential is frequently used to model binary liquids and glasses. In general there are six parameters ϵ_{AB} and σ_{AB} for the bond energies and the bond distances and an additional parameter for the composition. Usually two parameters are eliminated via the approximations $\epsilon_{AB} = (\epsilon_{AA} + \epsilon_{BB})/2$ and $\sigma_{AB} = \sqrt{\sigma_{AA}\sigma_{BB}}$ (Lorentz-Berthelot rule), but this is not always possible for solid phases.[10–12] The reason is that the bond lengths in solids are determined by geometric dis-

8   H.-R. Trebin et al.

tances, and the Lorentz-Berthelot rule would lead to internal stresses that
could distort or destroy the solid.

For glasses there are a number of special choices for the potential pa-
rameters which have been shown to avoid crystallization under ordinary
conditions.[13–15] For some of them, however, a crystalline ground state has
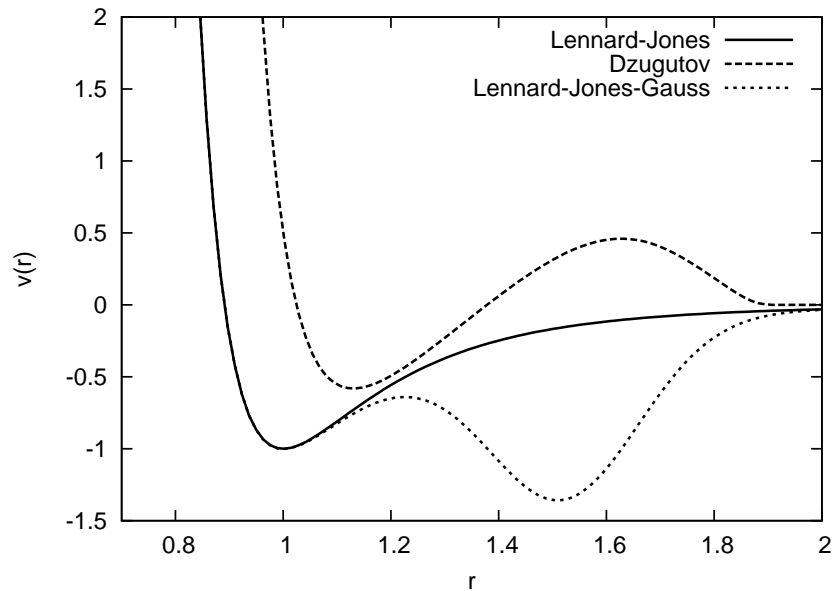resulted.[16–20]

Figure 1.1.   The Lennard-Jones, Dzugutov and Lennard-Jones-Gauss potential for
α=1.2, β^2=0.02 and r_0=1.52

1.3.2. *Dzugutov potentials*

The Dzugutov potential has been invented by M. Dzugutov for the descrip-
tion of monatomic metallic glasses (in contrast to covalent glasses).[21,22]
The problem with single-minima-interactions like Lennard-Jones or Morse
potentials $(v(r) = D(1 - e^{-a(r-r_0)})^2)$ is that if a sample is cooled from
the liquid state to the solid state it will *always* freeze into a close-packed
structure, either fcc or hcp or a mixture of both. Dzugutov's idea was to
prevent the crystalline order by introducing a maximum at the distance of

second nearest neighbours in close packed structures.

The Dzugutov pair potential is defined by the following equations (see Fig. 1.1):

$$\Phi(r) = \Phi_1 + \Phi_2, \tag{1.17}$$

$$\Phi_1 = A(r^{-m} - B)\exp\left(\frac{c}{r-a}\right), r < a, \tag{1.18}$$

$$\Phi_1 = 0, r \geq a, \tag{1.19}$$

$$\Phi_2 = B\exp\left(\frac{d}{r-b}\right), r < b, \tag{1.20}$$

$$\Phi_2 = 0, r \geq b, \tag{1.21}$$

with the parameters:

m	A	c	a	B	d	b
16	5.82	1.1	1.87	1.28	0.27	1.94

The special feature of the Dzugutov potential is a minimum at 1.13 of depth -0.581 followed by a maximum at 1.63 of height 0.460. The minimum has the same shape as in the case of the Lennard-Jones-potential. Past the maximum the potential goes to zero continously. The potential is cut off at a range of $r_c = 1.94$[a].

As a surprise came the discovery that the potential leads to dodecagonal quasicrystals if cooling is slow enough.[23] An evaluation of the pressure-temperature phase diagram of the potential leads to a rich variety of phases: at low temperatures and pressures the bcc phase has the lowest energy, and at high pressures the ground state is fcc.[24] Tetrahedrally close packed phases appear also, especially the σ phase, which can be considered as a low-order approximant of the quasicrystalline phases. It is assumed that the quasicrystalline phase is stabilized by entropy at low pressures and elevated temperatures. The Dzugutov potential does not possess separate liquid and gaseous phases due to its maximum and its rather short range.[25]

Since 1991 the potential has frequently been applied in the simulation of glasses, and it works quite well for this purpose.[26] Vibrational[27,28] and structural[29–31] properties have been studied extensively.

The global ground state of small Dzugutov clusters has been determined.[32,33] In contrast to the Lennard-Jones and Morse potentials the interaction strongly favors polytetrahedral clusters.

Diffusion has been studied[34] in monoatomic dodecagonal quasicrystals.

---

[a]Potential strength and range can be further scaled to adapt it to specific solids.

Below 60% of the melting temperature only single atomic jumps occur, while above that temperature diffusion is greatly enhanced and flips are found which rearrange the underlying quasicrystal tiling structure. More recently the potential has also been applied in shock wave simulations.[35,36] Phase transitions between crystalline phases and solitons have been observed. The results show similarities to shock waves in iron simulated with EAM potentials although the interaction has not been fitted to any specific material.

1.3.3. *Lennard-Jones-Gauss potentials*

Electronic energy considerations have shown that the general form of pair potentials in metals resembles a strongly repulsive core plus a decaying oscillatory Friedel term[37] (see also Sec. 1.4.1). The shape of the Dzugutov potential reproduces the first oscillation. The next natural step is the addition of a second minimum leading to a double-well potential. One possible choice is the Lennard-Jones-Gauss potential (Fig. 1.1) given by

$$V(r) = \frac{1}{r^{12}} - \frac{2}{r^6} - \alpha \exp\left(-\frac{(r-r_0)^2}{2\beta^2}\right). \tag{1.22}$$

It consists of a Lennard-Jones minimum of depth 1, positioned at $r = 1$ and a negative Gaussian of depth α and width β at $r = r_0$. Structure formation and dynamics can be studied as a function of the three parameters. At the moment the phase diagram of the system has only been calculated in two dimensions.[38] For $T = 0$, $P = 0$, and $\beta^2 = 0.02$ it is shown in Fig. 1.2 over the α-r_0 parameter space. A surprising variety of structures, four simple crystals (Hex1, Hex2, Sqa, and Rho) and five complex crystals (Pen, Xi, Sig1, Sig2, and Sig3) occur as stable ground states. The largest one (Xi) has 13 atoms per unit cell and a lattice constant about three times r_0, which is already remarkably complicated – at least for a monatomic crystal in two dimensions and a simple isotropic pair potential.

Simulations reveal, that the particle dynamics during crystal growth, but also in equilibrium crucially depends on the structural complexity. In addition to the usual vacancy and interstitial diffusion in simple phases, particle jumps (phason flips) are observed in the complex phases. They generate local tile rearrangements, but do not alter the long-range order. At elevated temperature the resulting entropic contribution to the free energy plays an important role in the thermodynamic stabilization. This is observed for example in the case of a reversible order-disorder transition
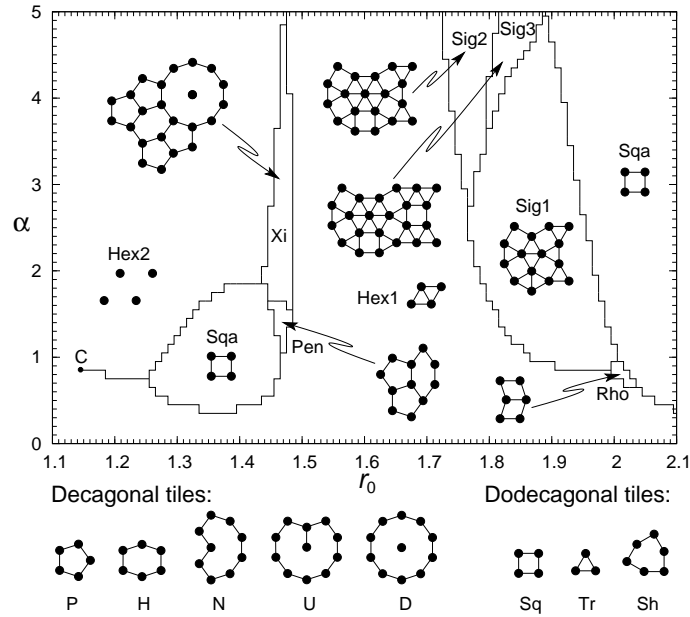
Figure 1.2.   Phase diagram of the Lennard-Jones-Gauss potential. Unit cell decorations of the crystals are depicted. For $r_0 \approx 1.47$ pentagonal local order and for $r_0 \approx 1.85$ dodecagonal local order is found. The tiles are basic building blocks of the complex phases.

between the low-temperature periodic crystal Xi and a high-temperature decagonal random tiling quasicrystal.[38]

By the choice Eq. (1.22) for the interaction potential two competing particle distances are introduced into the system. Depending on their ratio various local configurations can be favourable. If the most stable local configuration is not compatible with periodicity, structural complexity is a natural consequence. In fact, complexity seems to be closely related to the occurrence of two competing characteristic length scales also for real systems, where additionally the interplay of different atom species can play a role. An example are the binary Laves-phases, which are stabilized in a narrow range of the atom size ratio.

Note that the complex phases in Fig. 1.2 primarily appear in the region, where the second minimum is deeper than the first minimum, i.e. $\alpha > 1$. In realistic pair potentials the first minimum is often either degenerated to a shoulder or deeper than the second one. This might be a reason, why

complex phases are not found in elementary metals, at least under ambient external conditions. This is not true, however, for metalloid elements due to stronger angle-dependent multi-body contributions to the interaction. The phase β-boron with 105 atoms per unit cell, thermodynamically stable at high temperatures, is primarily built from icosahedrons arranged on a rhombohedral lattice.[39] Furthermore, complex phases are found quite frequently in many elemental metals at high pressures.[40] It is conceivable that shoulders in the interaction potential are increasingly significant under compression.

1.4. Realistic potentials

More realistic potentials can be obtained in essentially two ways, which are often applied in combination. One way is to derive an effective potential from a more fundamental theory, such as Density Functional Theory (DFT), by making a suitable series expansion, or by applying various physically motivated approximations, which naturally must depend on the nature of the system at hand (whether it is metallic, covalent, etc.). The other way is to choose a parametrized potential family, and to determine the parameters so that the potential correctly reproduces certain reference quantities, which can either be measured or computed ab-initio. The choice of the potential family is again dictated by the nature of the system, and its functional form is often inspired by approximations to DFT.

The first potentials of this kind had relatively few parameters and a functional form closely related to DFT. This often results in relatively complicated analytical formulae which are expensive to evaluate numerically. Moreover, it is difficult to verify the correctness of a program. Examples for such potentials are the original Finnis-Sinclair[41] and Embedded-Atom-Method (EAM) potentials[42–45] for metals, Tersoff potentials[46] for covalent solids, and generalizations of them like bond-order potentials,[47] and the modified EAM (MEAM) potentials.[48–50]

With the availability of an almost unlimited amount of ab-initio computed reference quantities which allow to fit a large number of potential parameters, it has become more convenient and also more efficient to use much larger potential families with completely free parameter functions. One example are the modern EAM or glue potentials, whose parameter functions no longer are required to have a functional form prescribed by DFT, but are freely fitted to reference quantities. Similarly, ADP potentials[51] (Angle Dependent Potentials) generalize in a sense the MEAM po-

tentials. They contain similar angle dependent terms, but have a simpler functional form at the expense of a larger number of potential parameters, and are much simpler and more efficient to evaluate.

In the following, we introduce in some more detail the Moriarty-Widom pair potentials directly derived from DFT, and the EAM and ADP potentials, whose parameter functions are determined by fitting to a data base of reference quantities.

1.4.1. *Moriarty–Widom Pair Potentials*

By a systematic series expansion of DFT into n-body terms, and by making various approximations, Moriarty and Widom[52,53] developed a family of potentials for aluminium-rich Al-TM (transition metal) alloys. Of course, n-body interactions with arbitrarily high n are not suitable for numerical simulations. Fortunately, it turns out that the complete interaction is already well approximated by the one- and two-body terms. At fixed volume, even the (density dependent) one-body term can be neglected. Only the higher-order terms of the TM-TM interactions give a non-negligible contribution, which can be approximated by an extra effective pair term not yet included in the expansion. Such an extra pair term could be fitted empirically to an ab-initio simulation of a decagonal quasicrystal.[54] The resulting effective pair potentials, an example of which is shown in Fig. 1.3, exhibit characteristic Friedel oscillations, which are believed to be important for the stabilization of complex crystals and quasicrystals. The potentials have been used very successfully for different kinds of simulations of decagonal quasicrystals, such as structure optimisation through total energy calculations,[55] or the simulation of aluminium diffusion in decagonal Al-Ni-Co.[56]

1.4.2. *Embedded Atom Method Potentials*

Pure pair potentials, even with optimally chosen parameter functions, cannot describe the interactions in a metal adequately. This holds true at least for relatively simple, short range potentials (note that the Moriarty-Widom potentials discussed above have long-range Friedel oscillations, which remedy part of the deficiencies). The problem is, that in a metal the interactions are density-dependent; one cannot simply add up the contributions of the different neighbours to the potential. In order to better mimic the physics of metallic cohesion, the so-called Embedded Atom Method (EAM) was introduced.[41–43,45] The corresponding potentials contain, in addition to a

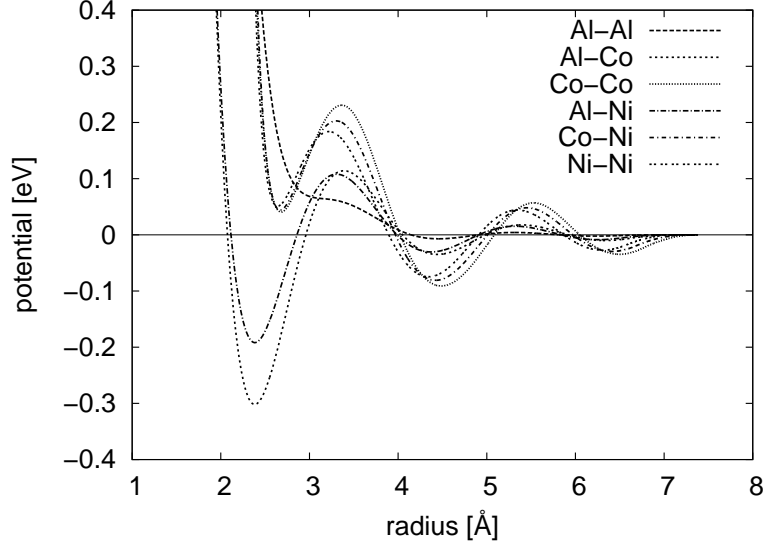14   *H.-R. Trebin et al.*

Figure 1.3.   Effective pair potentials for decagonal AlNiCo according to Moriarty and Widom[52,53]

conventional pair interaction, a density-dependent embedding term:

$$V = \sum_{i,j<i} \phi_{s_i s_j}(r_{ij}) + \sum_i U_{s_i}(n_i) \qquad \text{with} \quad n_i = \sum_{j \neq i} \rho_{s_j}(r_{ij}). \qquad (1.23)$$

The embedding term consists of a non-linear function $U_{s_i}(n_i)$, whose argument, the local density n_i at the position of atom i, is a sum of contributions from the neighbours j through a transfer function ρ_{s_j}. $U_{s_i}(n_i)$ yields the energy associated with placing atom i at the density n_i. This form was actually inspired by DFT, from where also the form of the embedding function was suggested. In modern versions, however, all parameter functions in Eq. (1.23) are freely optimized. This more general version is also known as glue potential.[44] EAM or glue potentials have been shown to describe the interactions in a metal much better than pair potentials.[44] Even though they contain many-body terms through the non-linearity of the embedding function, they are still relatively efficient to compute. Compared to pair potentials, a second loop over all neighbour pairs is required (one to compute n_i, another to compute the energy and the forces), so that the total effort is approximately doubled.

The EAM potential Eq. (1.23) has two gauge degrees of freedom, i.e.,

two sets of parameter changes which do not alter the physics of the potential:

$$\rho_s(r) \to \kappa \rho_s(r),$$
$$U_{s_i}(n_i) \to U_{s_i}\left(\frac{n_i}{\kappa}\right), \qquad (1.24)$$

and

$$\phi_{s_i s_j}(r) \to \phi_{s_i s_j}(r) + \lambda_{s_i}\rho_{s_j}(r) + \lambda_{s_j}\rho_{s_i}(r),$$
$$U_{s_i}(n_i) \to U_{s_i}(n_i) - \lambda_{s_i}n_i. \qquad (1.25)$$

According to Eq. (1.24), the units of the density n_i can be chosen arbitrarily. The transformation Eq. (1.25) states that certain energy contributions can be moved freely between the pair and the embedding term. An embedding function U which is linear in the density n can be gauged away completely. This also makes any separate interpretation of the pair potential part and the embedding term void; the two must be judged together. The latter degeneracy is usually lifted by choosing the gradients of the $U_i(n_i)$ to vanish at the average density for each atom type.

1.4.3. *Angular-Dependent Potentials (ADP)*

Neither pair nor EAM potentials contain any angle-dependent terms, wherefore they cannot be used for covalent systems. But even for certain metals, such terms cannot be completely neglected. This is likely to be true for metals having only a small number of valence electrons, or which are on the border of being metals. For such cases, Baskes[48,49] has proposed the Modified EAM (MEAM) potentials, which were later modified[50] once more by introducing a screening function. All variants involve relatively complicated analytical formulae, which are difficult to evaluate numerically. This is especially true for molecular dynamics, where not only the potential, but also its derivative is required. For this reason, implementations of MEAM are rarely available, and if they are, they are slow and not well suited for large-scale simulations.

Recently, however, Mishin et. al.[51] introduced a potential which contains essentially the same angle-dependend terms as the MEAM potential, but with a functionally much simpler form. They termed it ADP for Angle-Dependent Potential. Formally, ADP is an extension of EAM by further embedding terms:

$$V = \frac{1}{2}\sum_{i\neq j}\phi(r_{ij}) + \sum_i U(n_i) + \frac{1}{2}\sum_{i,\alpha}(\mu_i^\alpha)^2 + \frac{1}{2}\sum_{i,\alpha,\beta}(\lambda_i^{\alpha\beta})^2 - \frac{1}{6}\sum_i \nu_i^2. \quad (1.26)$$

The first two terms are the standard EAM potential (1.23). The third term measures the energy cost of a dipole distortion of an atomic environment, the fourth and the fifth term that of a quadrupole distortion. For this purpose, for each atom a net dipole distortion vector

$$\mu_i^\alpha = \sum_{j \neq i} u_{ij}(r_{ij}) r_{ij}^\alpha \tag{1.27}$$

and a quadrupole distortion tensor

$$\lambda_i^{\alpha\beta} = \sum_{j \neq i} w_{ij}(r_{ij}) r_{ij}^\alpha r_{ij}^\beta. \tag{1.28}$$

are computed. The last term in Eq. (1.26) compensates for the trace of $\lambda_i^{\alpha\beta}$:

$$\nu_i = \sum_\alpha \lambda_i^{\alpha\alpha}. \tag{1.29}$$

In the equations above, u_{ij} and w_{ij} are parameter functions which must be determined from reference data, and α and β represent cartesian coordinates x, y, or z. As the angle dependent terms occur only implicitly (in the squares of μ_i^α and $\lambda_i^{\alpha\beta}$) the computation of the ADP potential is algorithmically similar to EAM. It requires about twice as much computation time as EAM, and is thus at least two to three times faster than MEAM. Moreover, the program code is much simpler and more transparent. Also the expressions for the forces are fairly simple.[51]

1.5. Potential development with *potfit*

The reliability and predictive power of classical MD simulations depend crucially on the quality of the effective potentials employed. In the case of elementary solids, such potentials are usually obtained by adjusting a few potential parameters to optimally reproduce a set of reference data, which typically includes a number of experimental values like lattice constants, cohesive energies, or elastic constants, sometimes supplemented with ab-initio cohesive energies and stresses.[45] In the case of more complex systems with a large variety of local environments and many potential parameters to be determined, such an approach cannot help, however: there is simply not enough reference data available.

The force matching method[57] provides a way to construct physically justified potentials even under such circumstances. The idea is to compute forces, energies and stresses from first principles for a suitable selection of

small reference systems and to adjust the parameters of the potential to optimally reproduce them.

The force matching algorithm is implemented in the program *potfit*, the details of which have been described previously.[58] By separating the process of optimization from the form of the potential, *potfit* allows for maximal flexibility in the choice of potential model and parametrization.

1.5.1. *Algorithms*

potfit consists of two separate parts. The first one implements a particular parametrized potential model and calculates from a set of potential parameters ξ_i the target function that quantifies the deviations of the forces, stresses and energies from the reference values. Wrapped around is a second, potential independent part which implements a least square minimization module. As this part is completely independent of the potential model and just deals with the list of parameters ξ_i, it is fairly straightforward to change the parametrization of the potential (tabulated or analytic), or even to switch to a different potential model.

From a mathematical point of view, force matching is a basic optimization problem: There is a set of parameters ξ_i, a set of values $b_k(\xi_i)$ depending on them, and a set of reference values $b_{0,k}$ which the b_k have to match. This leads to the well-known method of least squares, where one tries to minimize the sum of squares of the deviations between the b_k and the $b_{0,k}$. In this case, the reference values can either be the components of the force vector $\vec{f}_{0,j}$ acting on each individual atom j, or global data $A_{0,k}$ like stresses, energies, or certain external constraints. It is helpful to measure the relative rather than the absolute deviations from the reference data, except for very small reference values. The least squares target function thus becomes

$$Z = Z_{\mathrm{F}} + Z_{\mathrm{C}}, \tag{1.30}$$

$$\text{with} \quad Z_{\mathrm{F}} = \sum_{j=1}^{N_A} \sum_{\alpha=x,y,z} W_j \frac{(f_{j_\alpha} - f_{0,j_\alpha})^2}{\vec{f}_{0,j}^2 + \varepsilon_j}, \tag{1.31}$$

$$\text{and} \quad Z_{\mathrm{C}} = \sum_{k=1}^{N_c} W_k \frac{(A_k - A_{0,k})^2}{A_{0,k}^2 + \varepsilon_k}, \tag{1.32}$$

where Z_F represents the contributions of the forces, and Z_C that of the global data. The (small and positive) ε_ℓ impose a lower bound on the denominators, thereby avoiding too an accurate fitting of small quantities

which are actually not known to such a precision. The W_l are the weights of the different terms. It proves useful for the fitting to give the total stresses and the cohesion energies an increased weight, although in principle they should be reproduced correctly already from the forces. Even if all forces are matched with a small deviation only, those deviations can add up in an unfortunate way when determining stresses, thus leading to potentials giving wrong elastic constants. Including global quantities in the fit with a sufficiently high weight supresses such undesired behaviour of the fitting process.

As the evaluation of the highly nonlinear target function Eq. (1.30) is computationally rather expensive, a careful choice of the minimization method has to be made. There are two algorithms in *potfit*. The first is a deterministic algorithm described by Powell,[59] which takes advantage of the form of the target function (which is a sum of squares). By re-using data obtained in previous function calls it arrives at the minimum faster than standard least squares algorithms. It also does not require any knowledge of the gradient of the target function.

The other minimization method implemented is a simulated annealing[60] algorithm proposed by Corana.[61] While the deterministic algorithm mentioned above will always find the closest *local* minimum, simulated annealing samples a larger part of the parameter space and thus has a chance to end up in a better minimum. The price to pay is a computational burdon which can be several orders of magnitude larger.

The basic Monte Carlo move is adding Gaussian-shaped bumps to the potential functions. The bump heights are normally distributed around zero, with a standard deviation adjusted so that on average half of the Monte Carlo steps are accepted. This ensures optimal progress: Neither are too many calculations wasted because the changes are too large to be accepted, nor are the steps too small to make rapid progress.

Generally, potential functions can be specified in various ways. They can either be given in analytic form, using a small number of free parameters, like for a Lennard-Jones potential, or in tabulated form together with an interpolation scheme for distances between the tabulation points. Whereas the parameters of an analytic potential can often be given a physical meaning, such an interpretation is usually not possible for tabulated potentials. On the other hand, an inappropriate form of an analytic potential may severely constrain the optimization, leading to a poor fit. For this reason, the functions are defined by tabulated values and spline interpolation, thus avoiding any bias introduced by an analytic potential. This choice results

in a relatively high number of potential parameters, compared to an analytic description of the potentials. This is not too big a problem, however: Force matching provides enough reference data to fit even a large number of parameters. The potential functions only need to be defined at pair distances r between a minimal distance $r_{\min}$ and a cutoff radius r_{cut}, where the function should go to zero smoothly.

1.5.2. *Implementation*

The program is parallelized using the standard Message Passing Interface (MPI[62]), simply by distributing the calculation of forces, energies and stresses in different configurations on several processes. Additionally, neighbour lists and lookup tables are used to speed up spline interpolation.

potfit was designed to cooperate closely with the first-principles code VASP[63,64] and with IMD,[4] our own classical MD code. VASP, which is a plane wave code implementing ultrasoft pseudopotentials and the Projector-Augmented Wave (PAW) method,[65,66] is used to compute the reference data for the force matching, whereas the resulting potentials are intended to be used with IMD. For this reason, *potfit* provides import and export filters for potentials and configurations to communicate with these programs. These filters are implemented as scripts, which can easily be modified to interface with other programs. All *potfit* input and output files are plain text files, so they can be manipulated without problems.

1.5.3. *Results and validation*

The correctness of *potfit* was verified by recovering a classical potential from reference data computed with that potential. This test succeeded perfectly for both a monatomic Lennard-Jones potential and a binary EAM potential. One should keep in mind, however, that reference data from ab-initio computations in general cannot be reproduced perfectly by any classical potential.

Although the potentials to be generated are intended for (aperiodic) quasicrystals and crystals with large unit cells, all reference structures have to be periodic crystals with unit cell sizes suitable for the ab-initio computation of the reference data. On the other hand, the reference structures should approximate the quasicrystal in the sense, that all their unit cells together accommodate all relevant structural motifs. To do so, they must be large enough. For instance, the quasicrystalline and related crystalline phases of Ca-Cd and Mg-Zn consist of packings of large icosahedral clusters

in different arrangements. Reference structures must be able to accomodate such clusters. A further constraint is, that the unit cell diameter must be larger than the range of potentials. Reference structures with 80–200 atoms represent a good compromise between these requirements.

Starting from a selection of basic reference structures, further ones are obtained by taking snapshots of MD simulations with model potentials at various temperatures and pressures. Also samples which were strained in different ways are included. For all these reference structures, the ab-initio forces, stresses and energies are determined with VASP, and a potential is fitted to reproduce these data. As reference energy, the cohesive energy is used, i.e., the energies of the constituent atoms are subtracted from the VASP energies. Instead of absolute cohesive energies one can also use the energy relative to some reference structure. Once a first version of the fitted potential is available, the MD snapshots can be replaced or complemented with better ones obtained with the new potential, and the procedure is iterated.

During the optimization, the target function Eq. (1.30) does not converge to zero, which indicates that quantum mechanical reality (taking density functional theory as reality) is not represented perfectly by the potential model used. The forces computed from the optimal potential typically differ by about 10% from the reference forces, which seems acceptable. For the energies and stresses a much higher agreement can be reached. Cohesion energy differences for instance can be reproduced with an accuracy better than 1%.

The generated potentials can then be used in molecular dynamics simulations to determine various material properties. Examples are described in Sec. 1.6 below.

It should be kept in mind that force-matched potentials will only work well in situations they have been trained to. Therefore, all local environments that might occur in the simulation should also be present in the set of reference configurations. Otherwise the results may not be reliable. Using a very broad selection of reference configurations will make the potential more *transferable*, making it usable for many different situations, e.g. for different phases of a given alloy. On the other hand, giving up some transferability may lead to a higher precision in special situations. By carefully constraining the variety of reference structures one may generate a potential that is much more precise in a specific situation than a general purpose potential, which was trained on a broader set of reference structures. The latter potential, on the other hand, will be more versatile, but less accurate

on average. Finding sufficiently many suitable reference structures might not always be trivial. For certain complex structure like quasicrystals, there may be only very few (if any) approximating periodic structures with small enough unit cell.

potfit does currently not use experimental data during force matching. The potentials are determined exclusively from ab-initio data, which means they cannot exceed the accuracy of the first principles calculations. While it is possible, in principle, to support also the comparison to experimental values, we decided against such an addition. For once, available experimental values can often not be calculated directly from the potentials, so determining them would considerably slow down the evaluation of the target function Eq. (1.30). Secondly, experimental values often also depend on the exact structure of the system, which in most cases is not completely known beforehand for complex structures, for instance due to fractional occupancies in the experimentally determined structure model. A better way to use experimental data is to test whether the newly generated potentials lead to structures that under MD simulation show the behaviour known from experiment.

It should be emphasized, however, that constructing potentials is still tedious and time-consuming. Potentials have to be thoroughly tested against quantities not included in the fit. In this process, candiate potentials often need to be rejected or refined. Many iterations of the fitting-validation cycle are usually required. It takes experience and skill to decide when a potential is finished and ready to be used for production, and for which conditions and systems it is suitable. *potfit* is only a tool that assists in this process. Flexibility and easy extensibility was one of the main design goals of *potfit*. While at present only pair and EAM potentials with tabulated potential functions are implemented in *potfit*, it would be easy to complement these by other potential models, or to add support for differently represented potential functions.

1.6. Simulations of physical properties

1.6.1. *Diffusion in d-Al-Ni-Co*

Aluminium is the majority element in many quasicrystals and expected to be the most mobile element, but due to the lack of suitable radio-tracers its diffusion properties are hardly accessible to experiment. Here, we investigate aluminium diffusion in decagonal Al-Ni-Co quasicrystals by molecular

H.-R. Trebin et al.

dynamics simulations. The calculations were carried out with newly developed EAM potentials[67] (see also Sec. 1.5).

The model structures of Ni-rich decagonal Al-Ni-Co ($Al_{72}Ni_{21}Co_9$) consists of an alternate stacking of two different layers which are decorations of the same hexagon-boat-star (HBS) tiling, resulting in a period of about 4Å.[68,69] We use a slightly modified variant determined in relaxation simulations, where it was found that the two innermost Al atoms in the star tiles prefer different positions, and also break the 4Å periodicity locally to an 8Å periodicity.[56] In the quasiperiodic plane the structure contains decagonal clusters which consist of 5, 7 or 8 Al atoms and 5, 3 or 2 Ni atoms.

Significant anisotropic diffusion of Al was observed at temperatures above 0.6 T_{melt}. It was found that the diffusion in the decagonal plane proceeds via mechanisms which are specific to quasicrystals. Of great importance are sites which tend to emit atoms, whereas other sites can absorb atoms. Chain processes occur, where the initial and the final positions are at these sites. As shown in Fig. 1.4, mobile Al atoms are located in the clusters with 7 or 8 Al atoms and within supertiles.

An important characteristic of this decagonal structure is that some Al positions are not localized, but there are regions of continuous Al density (Fig. 1.5). In the periodic direction, channels of continuous Al density spread through the structure. The diffusion in this direction runs via such channels. The diffusion mechanism is the direct position exchange of a column of atoms. In each period there are three atoms which are part of this column. With more than three periods the process is usually coupled with a jump process in the decagonal plane. An atom of the decagonal plane jumps into the diffusion channel, whereas another atom leaves the channel. In this case, only the atoms in-between diffuse along the channel. The diffusion channels are located in the centres of supertiles and in the centres of decagonal clusters which contain three atoms per period.

There are clearly more Al atoms which contribute to the diffusion in the decagonal plane than in the periodic direction, in which the diffusion is limited to the channels. However, since the mobility of Al atoms in the diffusion channels is significantly higher, the diffusion coefficients in the periodic direction are larger than those in the decagonal plane.

Time-averaged atom density maps calculated with ab-initio MD as well as classical MD with EAM potentials look very similar and confirm the existence of the continuous Al density regions. Furthermore, energy barriers calculated for specific diffusion processes using EAM potentials were validated in ab-inito calculations as well. The energy barriers determined in

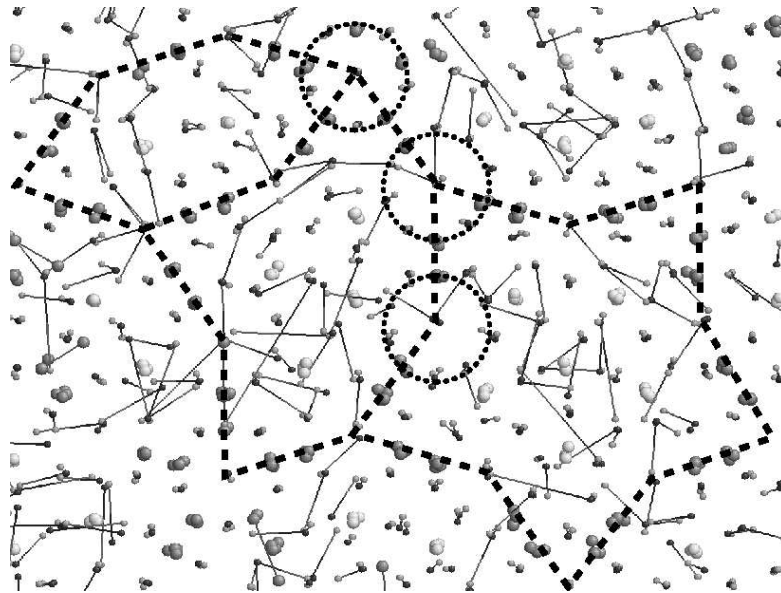*Simulation of complex metallic alloys*   23

Figure 1.4.   Diffusion processes in the decagonal plane. Dark grey, large: Ni; light grey, large: Co; dark grey, small: Al initial positions; light grey, small: Al positions after 100ps. Initial and final positions are connected. Dashed lines mark supertiles. Dotted circles mark three types of decagonal clusters, differing in the Ni content.

the periodic direction are about 0.3 eV per 8Å-period. For chain processes in the decagonal plane involving 3 atoms, an energy barrier of 0.5-2.5 eV was determined.[70]

1.6.2. *Dynamical structure factor*

The dynamical structure factor and other vibrational properties of a solid can in principle be derived from its eigenfrequencies and the corresponding eigenmodes. The eigenfrequencies are usually obtained in harmonic approximation: The system is relaxed to its ground state, around which the potential is expanded to second order to compute the dynamical matrix, which then is diagonalized numerically. An important advantage of this approach is that one can work with small systems (one unit cell) by sampling the Brillouin zone using Born-von-Karman boundary conditions. Computationally, it is much easier to diagonalize many small matrices instead of one big matrix for a large system. This makes the method usable even with ab-initio programs. Some MD or ab-initio programs directly provide the

24   *H.-R. Trebin et al.*

Figure 1.5.   Atom density map with regions of continous Al density. The lower part of the figure shows the marked stripe perpendicular to the periodic direction.

required derivatives of the forces. Otherwise it is always possible to take derivatives numerically. Unfortunately, there are also disadvantages. For complex structures, the ground state may not be very well defined, with many shallow minima, which can lead to numerical difficulties like negative eigenvalues of the dynamical matrix. Even more importantly, if there are low-energy structural transformations occurring, harmonic approximation may not be correct or accurate enough at higher temperatures.

Experimentally, phonons are usually studied by inelastic neutron scattering. These experiments measure certain correlation functions, which can be measured also in a molecular dynamics simulation. The advantage of such a procedure is the close resemblence to the experimental setup, so that

a direct comparison with experiment becomes possible. In particular, the simulation can be performed at the same temperature as the experiment, and is not restricted to harmonic approximation. In contrast to the dynamical matrix approach, however, it is not possible to use Born-von-Karman boundary conditions, so that large samples have to be simulated over long physical times, which excludes the use of ab-initio methods.

Most correlation functions of interest are actually time-dependent ones. As typical MD codes usually do not keep the whole MD trajectory in memory, they are best computed with some post-processing tool. nMoldyn[71] is such a post-processor. It is freely available and has been written exactly for the purpose of computing correlation functions related to neutron scattering experiments. nMoldyn uses as input the entire MD trajectory of the system, with all atom positions and velocities. For many MD programs, converters to the input format of nMoldyn exist. There is one problem, however: a long trajectory of a large system represents a huge amount of data. Note that if the Brillouin zone of a complex crystal phase with large unit cell shall be sampled with adequate accuracy, then a large system has to be simulated, and in order to obtain a reasonable frequency resolution, long trajectories are required. For one-particle correlation functions (self-correlations), where correlations of the properties of a particle with its own history are averaged over the system, one can restrict the trajectory to a representative subset of the particles, e.g. those in one unit cell. This trick can be used e.g. for the velocity auto-correlation, whose Fourier transform is the vibrational density of states.[71]

For collective correlation functions however, such an approach is not possible. Among those, the most interesting is the dynamical structure factor, which consists of a coherent and an incoherent part. The incoherent part is a one-particle correlation function and provides only a relatively smooth background. Interesting structural information is mostly contained in the (collective) coherent part, which is given by the Fourier transform of the coherent intermediate scattering function:

$$\mathcal{F}^c(q,t) = \frac{1}{N} \sum_{i,j} b_i^c b_j^c \langle \exp(-iq \cdot r_i(0)) \exp(iq \cdot r_j(t)) \rangle \tag{1.33}$$

$$= \frac{1}{N} \langle f(q,0)\overline{f(q,t)} \rangle = \frac{1}{N} \langle f(q,t_0)\overline{f(q,t+t_0)} \rangle_{t_0}, \tag{1.34}$$
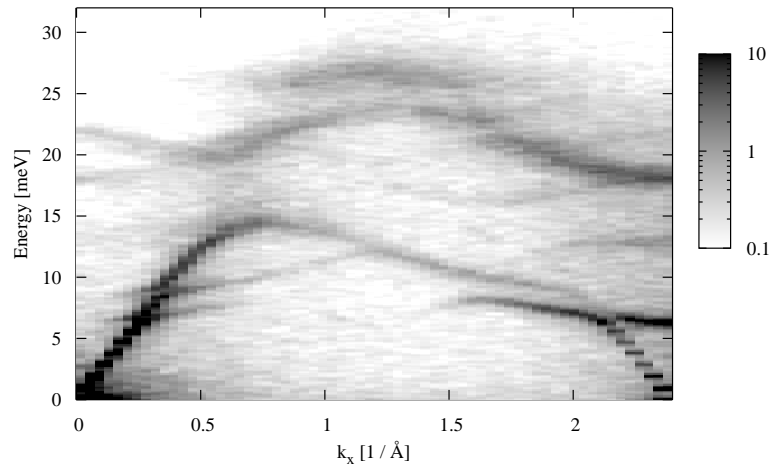
$$f(q,t) = \sum_i b_i^c \exp(-iq \cdot r_i(t)). \tag{1.35}$$

Figure 1.6.   Coherent part of the dynamical structure factor (longitudinal polarisation) for the Laves phase of $MgZn_2$.

Here, b_i^c is the coherent Neutron scattering amplitude. As we can see, for a fixed wave vector q the coherent intermediate scattering function $\mathcal{F}^c(q,t)$ is the autocorrelation of the time series $f(q,t)$, which can be measured for a selection of interesting values of q, say those on a suitable path in the Brillouin zone. Writing the time series $f(q,t)$ for a few hundred values of q produces much less data than the whole trajectory of all particles. From that data, it is then easy to compute the Fourier transform of its autocorrelation via the fast Fourier transform method,[71] which is done with a simple post-processor. As an example, we show in Fig. 1.6 the dynamical structure factor for longitudinal polarisation of the Laves phase of $MgZn_2$, determined with EAM potentials constructed with *potfit*,[58] as described in Sec. 1.5.

1.6.3.   *Cracks in NbCr₂*

By stretching a specimen, elastic energy is stored in the system. When a crack moves through such a strained brittle solid, free surfaces are generated. Thus, crack propagation should be possible, if the elastic energy is

sufficient for the generation of new fracture surfaces. It is evident from this so-called Griffith criterion,[72] that cleavage should probably occur on planes of lowest surface energy. However, this global thermodynamic picture does not take into account the discrete, atomistic nature of matter. Atomic bonds break at the crack tip. Their arrangement and individual strength can vary on different planes. From model calculations[73] it is known that cracks indeed can be stable for loads that lie well above the Griffith value. This is due to the fact that breaking bonds costs a high amount of energy locally. The crack can therefore be trapped by the lattice. To overcome this barrier, the energy for crack propagation now also has to be higher than the value coming only from the generation of flat surfaces. As a consequence, fracture surfaces are not necessarily those of lowest energy or lowest roughness (see e.g. Rösch et al.[74,75]). To investigate the influence of the lattice-trapping[73] effect on cleavage at low temperatures, we perform molecular dynamics simulations on the Friauf-Laves phase $NbCr_2$.

The EAM potentials for this compound were generated using the force-matching method as described in Sec. 1.5. Ab-initio reference data on deformed samples as well as on systems with free surfaces has been included in the fit. The lattice constant, the elastic constants, and the melting temperature obtained with these interactions agree with experimental findings and ab-initio results.[76] The relaxation of atoms at free surfaces and the surface energy are also reproduced well.[76]

The Friauf-Laves phases[77–80] form the largest subset of topologically close-packed intermetallic compounds.[81] They frequently combine interesting properties like high melting point, high temperature strength, and low density. However, their applications are limited by an extreme brittleness at low and ambient temperatures. In C15 $NbCr_2$ the Cr atoms sit on a tetrahedral network, whereas the Nb atoms form a diamond lattice. A cubic cell contains 24 basis atoms. On the other hand, the Friauf-Laves phases can be described as a stacking of layers (see e.g. Livingston[82] and Hazzledine et al.[83]) along the [111] direction.

We insert an atomically sharp seed crack in a relaxed specimen between (111) planes of lowest surface energy. The samples consist of about five million atoms. Periodic boundary conditions are applied parallel to the crack front. For the other directions, atoms in the outermost boundary layers are held fixed. The system is uniaxially strained perpendicular to the crack plane up to the Griffith load and relaxed. The crack then is further loaded by scaling the resulting displacement field at low temperature. Sound waves emitted by the propagating crack are damped away by the

H.-R. Trebin et al.

applied molecular dynamics scheme.[84]

From pure energy considerations, the crack propagation direction on one and the same plane should not change fracture behaviour. The required surface energy stays constant. From an atomistic viewpoint, however, the number and orientation of bonds that are approached by a propagating crack front may differ. In fact, this influence can be observed for two different propagation directions on a (111) plane in $NbCr_2$.

Geometrically scanned fracture surfaces for cracks that propagated along a $[2\bar{1}\bar{1}]$ and a $[0\bar{1}1]$ direction are given in Fig. 1.7. The flat seed crack has been built-in on the left. The energy release rate has been increased to about 170% of the Griffith value to allow both cracks to overcome the lattice-trapped state and to propagate with constant velocity. The crack moving in $[2\bar{1}\bar{1}]$ direction initially climbs up one atomic layer. Brittle cleavage fracture on this plane then is observed. The surplus of energy causes several point defects (see Fig. 1.7, top). In contrast, the crack propagating along a $[0\bar{1}1]$ axis causes a rougher surface (see Fig. 1.7, bottom). It seems that the crack could not decide whether to stay on the initial cleavage plane or to move up one atomic layer. The energy of the generated surfaces is in both cases higher than the energy of the initial flat cleavage planes ($[2\bar{1}\bar{1}]$: +13%, $[0\bar{1}1]$: +28%). So, the main part of the energy surplus goes into radiation. Rougher surfaces cost more energy to generate. The associated crack also travels slower ($[2\bar{1}\bar{1}]$: 1.05 km/s, $[0\bar{1}1]$: 0.76 km/s). Thus, macroscopic properties differ for the two propagation directions. This reveals that computer experiments on an atomic scale are necessary to simulate and to understand fracture properly.

The crack travelling in $[2\bar{1}\bar{1}]$ direction changes the initial cleavage plane for diverse applied loads always as shown in Fig. 1.7. Flat cuts at both heights cost the same amount of energy. The height thus could be chosen randomly. However, a crack shifted up one atomic layer does not deviate from this plane (see Fig. 1.8). The initial lattice trapping for the shifted crack is somewhat lower (an energy surplus of about 32% instead of 44% allows propagation). Thus, the bonds that are approached first at the crack tip even seem to select the cleavage plane. This subtle detail again emphasizes the importance of the lattice-trapping effect. The molecular dynamics simulations show, that fracture is determined by processes on the atomic level. These define whether, where, and how a crack propagates.
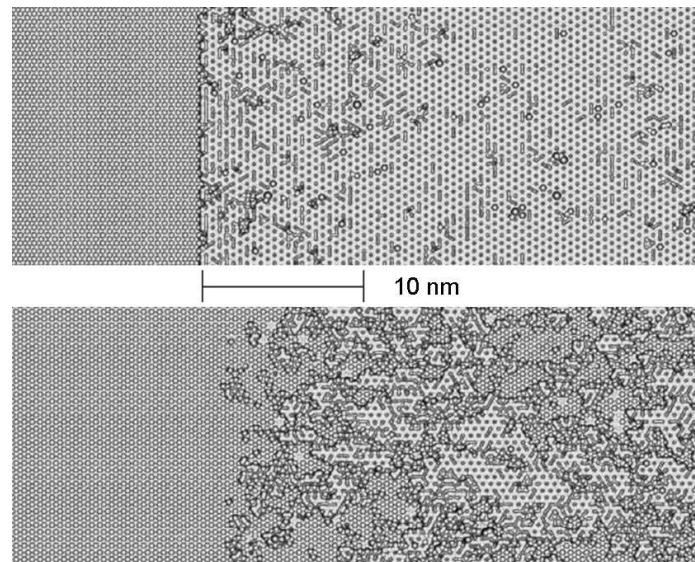
Figure 1.7.   Sections of (111) fracture surfaces geometrically scanned with a Nb atom. The crack propagated in $[2\bar{1}\bar{1}]$ (top) and in $[0\bar{1}1]$ direction (bottom).
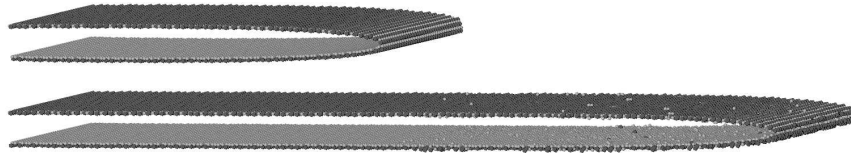

Figure 1.8.   Atoms forming the fracture surfaces of the shifted crack. Only particles with low coordination number are displayed. The seed crack (top) propagates smoothly on the initial height (bottom: after 0.1 ns).

1.6.4. *Order-disorder transition in CaCd$_6$*

CaCd$_6$ can be understood as the cubic 1/1-approximant of the thermodynamically stable Ca-Cd icosahedral quasicrystal.[85,86] Both the quasicrystal and the complex periodic phases can be described as packings of essentially identical clusters with some additional glue atoms in-between.[87,88] In the cubic CaCd$_6$ phase, these clusters are arranged on a bcc lattice. The clusters each contain a total of 66 atoms in four shells: A Cd tetrahedron is believed to be the central shell, surrounded by a Cd dodecahedron, a Ca

icosahedron and a Cd icosidodecahedron.[89] While the outer three shells
are icosahedrally symmetric, this symmetry is broken by the innermost
tetrahedron.

The cubic 1/1-approximant $CaCd_6$ (and the isostructural $YbCd_6$) show
an order-disorder phase transition at 100 K (and 110 K, respectively), which
is attributed to a reordering or disordering of the orientations of the tetra-
hedral central shell. At the phase transition temperature, there is a peak
in the heat capacity and a discontinuity of the electrical conductivity.[90,91]

From X-ray diffraction, Gómez and Lidin[89] concluded that the central
shell is a distorted tetrahedron suffering from two types of disorder. The
first is a 90° rotational disorder along the twofold axis of the tetrahedron,
which leads to a cube with alternately occupied corners. The second type
of disorder is a triple split of the tetrahedron corner atoms that arises when
the threefold rotational axis does not coincide with the body diagonal of
the cubic unit cell. These two types of disorder combined lead to 24 pos-
sible positions for four tetrahedral Cd atoms in each cluster's central shell,
as shown in Fig. 1.9(a). Based on this proposal, Nozawa and Ishii used
ab-initio methods to compare the energies of structures with different tetra-
hedron shapes and orientations.[92] However, the computational demands of
these methods make a similar treatment of larger supercells impossible.

Simulations with effective potentials turned out to be much better suited
to this task.[93] The *potfit*[58] program (Sec. 1.5) was used to create EAM
potentials for Ca-Cd, with the help of which the precise structure and or-
dering of the innermost CaCd cluster shell could be analyzed in a level of
detail that is inaccessible to ab-initio methods. To study the stability of
the Gómez-Lidin tetrahedra[89] as innermost shells, one generates all pos-
sible combinations of orientations of the tetrahedra in a cubic cell with
two clusters and relaxes these structures to the nearest energy minimum.
The resulting relaxed structures have six different energies in total, differ-
ing maximally by 0.17 meV/atom. The relaxed tetrahedra are all identical
(up to symmetry), the energy difference coming from the different relative
orientations of the two tetrahedra. This ideal tetrahedron is not equal to
the Gómez-Lidin one, however. Each atom relaxes in a specific way (two
atoms by 0.29Å, the other two by 0.17Å) to new tetrahedron corners, with-
out further symmetry breaking. The number of distinct ideal tetrahedra
therefore is still twelve, like the number of Gómez-Lidin tetrahedra, but
the total number of possible corner positions has doubled. In Fig. 1.9(b),
the new positions of a sample tetrahedron are shown in black, while the
medium gray cirles signify the original Gómez-Lidin positions. The light

Simulation of complex metallic alloys   31

gray positions are occupied by atoms belonging to rotated tetrahedra. The relaxation simulations also show that the surrounding shells of the clusters are strongly deformed by the inner tetrahedron. The stability of the ideal cluster has been verified also with ab-initio relaxations.

(a) Potential locations of the Cd tetrahedral atoms according to Gómez and Lidin.

(b) Improved tetrahedron. For an explanation, see text.
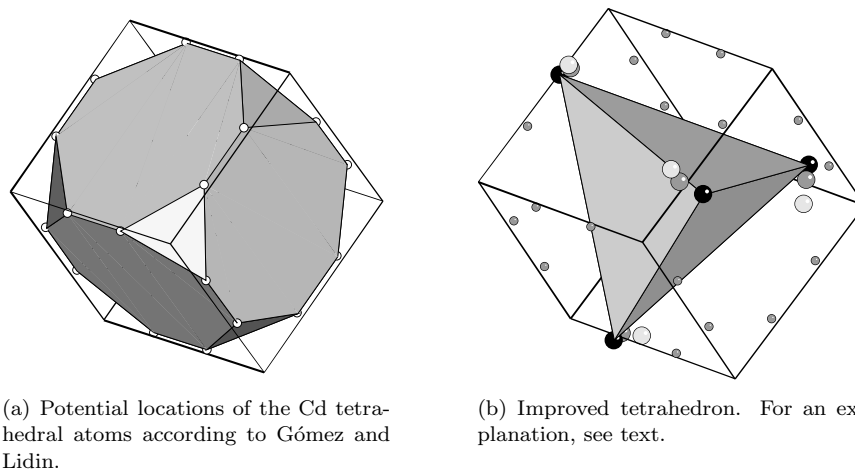
Figure 1.9.   Configuration of the Ca-Cd tetrahedron.

In a second step, finite temperature MD simulations were performed with a larger sample, consisting of $5 \times 5 \times 5$ cubic unit cells (250 clusters). These simulations show that, starting from an ordered low-temperature state, the tetrahedron orientations start to change at around 100 K, and even a few non-ideal tetrahedra show up. It was not possible, however, to see any clear sign of the expected phase transition, like a peak in the heat capacity or a jump in the inner energy, probably due to the bad statistics. A further step in our modelling of the interactions is therefore required.

In order to obtain better statistics, the number of degrees of freedom needs to be reduced. All clusters in low temperature states apparently have the same innermost shells in the form of the ideal tetrahedron introduced above, which occurs in twelve different orientations. One then can set up an effective hamiltonian modelling the interactions between neighbouring clusters via induced deformations of the outer shells. Neighbouring clusters can be in contact along two-fold or three-fold directions. Taking into account the different orientations of the inner tetrahedra at both ends of a bond, there are, up to symmetry, 26 types of 2-fold bonds and 16 types

of 3-fold bonds. Each bond of type α contributes an energy E_α to the hamiltonian.

The energies E_α can be determined by fitting to energies obtained in MD relaxations of supercells containing up to 64 clusters with randomly oriented tetrahedra. The cluster hamiltonian so derived can now be used in extensive Monte Carlo simulations. With a sample of $4 \times 4 \times 4$ unit cells containing 128 clusters, the internal energy as a function of temperature was determined,[93] which shows a sharp jump at about 89 K (Fig. 1.10), not far from the experimental transition temperature of 100 K.[91] This energy jump ΔE corresponds to an entropy jump $\Delta E/k_B T_0$ of roughly $1 k_B$ per cluster, which is about twice the amount estimated in Ref. 90.
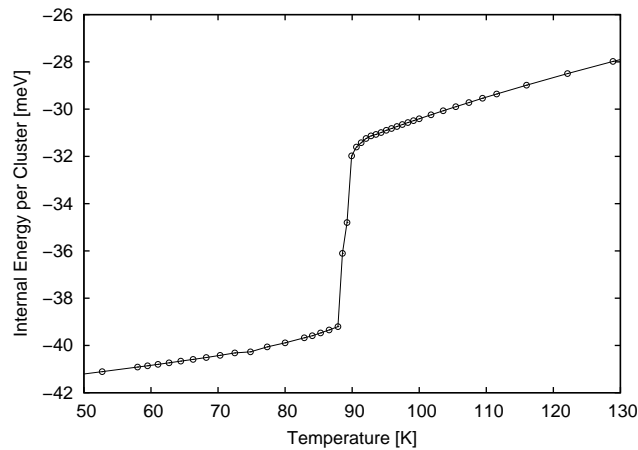

Figure 1.10.   Internal energy as a function of temperature for the effective cluster hamiltonian. A sharp jump is displayed at about 89 K.[93]

1.7. Conclusions

The molecular dynamics method allows to simulate a large variety of material properties and dynamical processes at the atomistic level. For complex materials and inhomogeneous systems with phase or grain boundaries and large defects, such a level of detail is indeed necessary. With classical effective potentials and large parallel computers, it is possible to routinely simulate systems with linear sizes exceeding 100Å, thus reaching well into the nano-domain. Even though classical potentials may seem to be a gross

Simulation of complex metallic alloys   33

approximation to the quantum-mechanical reality, with a well selected potential model (depending on the system type) and with carefully adjusted potential parameters, it is possible to perform simulations with high accuracy and reliability. This can be achieved by fitting the potential parameters to data obtained in quantum-mechanical calculations, thus making quantum-mechanical information available also to classical simulations.

In many situations, however, system sizes of 100Å and time spans of a few nanoseconds may still be far too small. But even in such cases, it is possible to use results of molecular dynamics simulations to determine parameters of higher level theories, such as continuum models, or effective models where part of the degrees of freedom have been integrated out, like models used in Monte Carlo simulations. Molecular dynamics therefore provides the basis also for those higher level theories, and is an essential ingredient for any multi-scale modelling of matter.

References

1. M. P. Allen and D. J. Tildesley, *Computer Simulation of Liquids.* (Clarendon Press, Oxford, 1992).
2. D. Frenkel and B. Smit, *Understanding molecular simulation: from algorithms to applications.* (San Diego: Academic Press, 2003).
3. D. C. Rapaport, *The Art of Molecular Dynamics Simulation.* Second Edition, (Cambridge University Press, 2004).
4. J. Stadler, R. Mikulla, and H.-R. Trebin, IMD: a software package for molecular dynamics studies on parallel computers, *Int. J. Mod. Phys. C.* **8**(5), 1131–1140, (1997). `http://www.itap.physik.uni-stuttgart.de/~imd/`.
5. F. Gähler and K. Benkert. Atomistic simulations on scalar and vector computers. In eds. M. Resch, T. Bönisch, K. Benkert, T. Furui, Y. Seo, and W. Bez, *High Performance Computing on Vector Systems*, p. 173. Springer, (2006). ISBN 3–540–29124–5.
6. F. F. Abraham, Computational statistical mechanics. Methodology, applications and supercomputing., *Adv. Phys.* **35**, 1–111, (1986).
7. F. H. Stillinger, Lattice sum and their phase diagram implications for the classical Lennard-Jones model., *J. Chem. Phys.* **115**, 5208–5212, (2001).
8. M. A. Barroso and A. L. Ferreira, Solid-fluid coexistence of the lennard-jones system from absolute free energy calculations, *J. Chem. Phys.* **116**, 7145–7150, (2002).
9. M. A. van der Hoef, Free energy of the Lennard-Jones solid, *J. Chem. Phys.* **113**, 8142–8148, (2000).
10. J. Roth, R. Schilling, and H.-R. Trebin, Stability of monoatomic and diatomic quasicrystals and the influence of noise, *Phys. Rev. B.* **41**, 2735–2747, (1990).
11. J. W. Roth, R. Schilling, and H.-R. Trebin, Nucleation of quasicrystals by

rapid cooling of a binary melt: A molecular-dynamics study, *Phys. Rev. B.* **51**(22), 15833–15840, (1995).

12. J. Roth and Ch.Henley, A new binary decagonal Frank-Kasper quasicrystal phase, *Phil. Mag. A.* **75**, 861–887, (1997).

13. W. Kob and H. C. Andersen, Kinetic lattice-gas model of cage effects in high-density liquids and a test of mode-coupling theory of the ideal-glass transition, *Phys. Rev. E.* **48**(6), 4364–4377, (1993).

14. W. Kob and H. Anderson, Testing mode-coupling thoery for a supercooled binary Lennard-Jones mixture: The van Hove correlation function, *Phys. Rev. E.* **51**(5), 4626–4641, (1995).

15. W. Kob and H. C. Anderson, Testing mode-coupling theory for a super-cooled binary lennard-jones mixture. ii. intermediate scattering function and dynamic susceptibility, *Phys. Rev. E.* **52**(4), 4134–4153, (1995).

16. M. J. Vlot, H. E. A. Huitema, A. de Vooys, and J. P. van der Eerden, Crystal structures of symmetric Lennard-Jones mixtures, *J. Chem. Phys.* **107**, 4345–4349, (2003).

17. M. Hitchcock and C. K. Hall, Solid-liquid phase equilibrium for binary lennard-jones mixtures, *J. Chem. Phys.* **110**, 11433–11444, (1999).

18. T. F. Middleton, J. Hernández-Rojas, P. N. Mortenson, and D. J. Wales, Crystals of binary Lennard-Jones solids, *Phys. Rev. B.* **64**, 184201, (2001).

19. J. R. Fernández and P. Harrowell, Crystal phases of a glass-forming Lennard-Jones mixture, *Phys. Rev. E.* **67**, 11403, (2003).

20. J. R. Fernández and P. Harrowell, Ordered binary crystal phases in Lennard-Jones mixtures, *J. Chem. Phys.* **120**, 9222–9232, (2004).

21. M. Dzugutov and U. Dahlborg, Molecular dynamics study of the coherent density correlation function in a supercooled simple one-component liquid, *J. Non-Cryst. Solids.* **131**, 62–65, (1991).

22. M. Dzugutov, Glass formation in a simple monoatomic liquid with icosahe-dral inherent local order, *Phys. Rev. A.* **46**, R2984 R2987, (1992).

23. M. Dzugutov, Formation of a dodecagonal quasicrystalline phase in a simple monatomic liquid, *Phys. Rev. Lett.* **70**(19), 2924–2927, (1993).

24. J. Roth and A. Denton, Solid phase structures for the Dzugutov pair poten-tial, *Phys. Rev. E.* **61**, 6845–6857, (2000).

25. J. Roth, The fluid-solid transition of Dzugutov's potential, *Eur. Phys. J. B.* **14**, 449–458, (2000).

26. M. Dzugutov, S. I. Simdyankin, and F. H. Zetterling, Decoupling of diffusion from structural relaxation and spatial heterogeneity in a supercooled simple liquid, *Phys. Rev. Lett.* **89**, 195701, (2002).

27. S. I. Simdyankin, S. N. Taraskin, M. Dzugutov, and S. R. Elliott, Vibrational properties of the one-component sigma phase, *Phys. Rev. B.* **62**, 3223–3231, (2000).

28. S. I. Simdyankin, S. N. Taraskin, M. Elenius, S. R. Elliott, and M. Dzugutov, Nature of vibrational eigenmodes in topologically disordered solids, *Phys. Rev. B.* **65**, 104302, (2002).

29. T. Mattila, R. M. Nieminen, and M. Dzugutov, Simulation of radiation-induced structural transformation in amorphous metals, *Phys. Rev. B.* **53**

(1), 192–200, (1996).

30. B. Sadigh, M. Dzugutov, and S. R. Elliott, Vacancy ordering and medium-range structure in a simple monatomic liquid, *Phys. Rev. B.* **59**, 1–4, (1999).

31. S. I. Simdyankin, M. Dzugutov, S. N. Taraskin, and S. R. Elliott, Connection between vibrational dynamics and topological order in simple glasses, *Phys. Rev. B.* **63**, 184301, (2001).

32. J. P. K. Doye, D. J. Wales, and S. I. Simdyankin, Global optimization and the energy landscapes of dzugutov clusters, *Faraday Discuss.* **118**, 159–170, (2001).

33. J. P. K. Doye and D. J. Wales, Polytetrahedral clusters, *Phys. Rev. Lett.* **86**, 5719–5772, (2001).

34. J. Roth and F. Gähler, Self-diffusion in dodecagonal quasicrystals, *Eur. Phys. J. B.* **6**, 425–455, (1998).

35. J. Roth, Shock waves in materials with Dzugutov-potential interactions, *Phys. Rev. B.* **72**, 014125, (2005).

36. J. Roth, ω-phase and solitary waves induced by shock compression of bcc crystals, *Phys. Rev. B.* **72**, 014126, (2005).

37. J. Hafner, *From Hamiltonians to Phase Diagrams.* (Springer-Verlag, Berlin, 1987).

38. M. Engel and H.-R. Trebin, Self-assembly of monatomic complex crystals and quasicrystals with a double-well interaction potential, *Accepted by Phys. Rev. Lett.* (2007).

39. J. Dondhue, *The Structures of the Elements.* (John Wiley and Sons, New York, 1974).

40. M. I. McMahon and R. J. Nelmes, High-pressure structures and phase transformations in elemental metals, *Chem. Soc. Rev.* **35**, 943–963, (2006).

41. M. W. Finnis and J. E. Sinclair, A simple empirical n-body potential for transition metals, *Phil. Mag. A.* **50**(1), 45–55, (1984).

42. M. S. Daw and M. I. Baskes, Semiempirical, Quantum Mechanical Calculation of Hydrogen Embrittlement in Metals, *Phys. Rev. Lett.* **50**(17), 1285–1288, (1983).

43. M. S. Daw and M. I. Baskes, Embedded-atom method: Derivation and application to impurities, surfaces, and other defects in metals, *Phys. Rev. B.* **29**(12), 6443–6453, (1984).

44. F. Ercolessi, M. Parrinello, and E. Tosatti, Simulation of gold in the glue model, *Phil. Mag. A.* **58**(1), 213–226, (1988).

45. M. S. Daw, S. M. Foiles, and M. I. Baskes, The embedded-atom method: a review of theory and applications, *Mater. Sci. Rep.* **9**(7–8), 251–310, (1993).

46. J. Tersoff, Modeling solid-state chemistry: Interatomic potentials for multi-component systems, *Phys. Rev. B.* **39**(8), 5566–5568, (1989).

47. D. G. Pettifor, *From Exact to Approximate Theory: The Tight Binding Bond Model and Many-Body Potentials*, In eds. R. M. Nieminen, M. J. Puska, and M. J. Manninen, *Many-Atom Interactions in Solids*, vol. 48, *Springer Proceedings in Physics*, pp. 64–84. Springer-Verlag, (1990).

48. M. I. Baskes, Application of the Embedded-Atom Method to Covalent Materials: A Semiempirical Potential for Silicon, *Phys. Rev. Lett.* **59**(23), 2666–

2669, (1987).

49. M. I. Baskes, Modified embedded-atom potentials for cubic materials and impurities, *Phys. Rev. B.* **46**(5), 2727–2742, (1992).

50. M. I. Baskes, Determination of modified embedded atom method parameters for nickel, *Mater. Chem. Phys.* **50**, 152–158, (1997).

51. Y. Mishin, M. J. Mehl, and D. A. Papaconstantopoulos, Phase stability in the Fe-Ni system: Investigation by first-principles calculations and atomistic simulations, *Acta Mater.* **53**(15), 4029–4041, (2005).

52. J. A. Moriarty and M. Widom, First-principles interatomic potentials for transition-metal aluminides: Theory and trends across the 3d series, *Phys. Rev. B.* **56**(13), 7905–7917, (1997).

53. M. Widom, I. Al-Lehyani, and J. A. Moriarty, First-principles interatomic potentials for transition-metal aluminides. III. Extension to ternary phase diagrams, *Phys. Rev. B.* **62**, 3648–3657, (2000).

54. I. Al-Lehyani, M. Widom, Y. Wang, N. Moghadam, G. M. Stocks, and J. A. Moriarty, Transition-metal interactions in aluminum-rich intermetallics, *Phys. Rev. B.* **64**, 075109, (2001).

55. M. Mihalkovič, I. Al-Lehyani, E. Cockayne, C. L. Henley, N. Moghadam, J. A. Moriarty, Y. Wang, and M. Widom, Total-energy-based prediction of a quasicrystal structure, *Phys. Rev. B.* **65**, 104205, (2002).

56. S. Hocker and F. Gähler, Aluminium diffusion in decagonal quasicrystals, *Phys. Rev. Lett.* **93**(7), 075901, (2004).

57. F. Ercolessi and J. B. Adams, Interatomic Potentials from First-Principles Calculations: the Force-Matching Method., *Europhys. Lett.* **26**(8), 583–588, (1994).

58. P. Brommer and F. Gähler, Potfit: effective potentials from ab-initio data, *Modelling Simul. Mater. Sci. Eng.* **15**(3), 295–304, (2007). `http://www.itap.physik.uni-stuttgart.de/~imd/potfit/`.

59. M. J. D. Powell, A method for minimizing a sum of squares of non-linear functions without calculating derivatives, *Comp. J.* **7**(4), 303–307, (1965).

60. S. Kirkpatrick, C. D. Gelatt, and M. P. Vecci, Optimization by simulated annealing, *Science.* **220**(4598), 671–680, (1983).

61. A. Corana, M. Marchesi, C. Martini, and S. Ridella, Minimizing Multimodal Functions of Continuous Variables with the "Simulated Annealing" Algorithm, *ACM Trans. Math. Soft.* **13**(3), 262–280, (1987).

62. W. Gropp, E. Lusk, and A. Skjellum, *Using MPI - 2nd Edition.* (The MIT Press, 1999). ISBN 0–262–57132–3.

63. G. Kresse and J. Hafner, *Ab initio* molecular dynamics for liquid metals, *Phys. Rev. B.* **47**(1), 558–561, (1993).

64. G. Kresse and J. Furthmüller, Efficient iterative schemes for *ab initio* total-energy calculations using a plane wave basis set, *Phys. Rev. B.* **54**(16), 11169–11186, (1996).

65. P. E. Blöchl, Projector augmented-wave method, *Phys. Rev. B.* **50**(24), 17953–17979, (1994).

66. G. Kresse and D. Joubert, From ultrasoft pseudopotentials to the projector augmented-wave method, *Phys. Rev. B.* **59**(3), 1758–1775, (1999).

67. P. Brommer and F. Gähler, Effective potentials for quasicrystals from ab-initio data, *Phil. Mag.* **86**(6–8), 753–758, (2006).

68. M. Mihalkovič, I. Al-Lehyani, E. Cockayne, C. L. Henley, N. Moghadam, J. A. Moriarty, Y. Wang, and M. Widom, Total-energy-based prediction of a quasicrystal structure, *Phys. Rev. B.* **65**, 104205, (2002).

69. E. Cockayne and M. Widom, Ternary model of an Al-Cu-Co decagonal quasicrystal, *Phys. Rev. Lett.* **81**, 598, (1998).

70. S. Hocker, F. Gähler, and P. Brommer, Molecular dynamics simulation of aluminium diffusion in decagonal quasicrystals, *Phil. Mag.* **86**(6–8), 1051–1057, (2006).

71. T. Róg, K. Murzyn, K. Hinsen, and G. R. Kneller, nMoldyn: A program package for a neutron scattering oriented analysis of molecular dynamics simulations, *J. Comput. Chem.* **24**, 657–667, (2003). `http://dirac.cnrs-orleans.fr/nMOLDYN/index.html`.

72. A. A. Griffith, The phenomena of rupture and flow in solids, *Philos. Trans. R. Soc. London, Ser. A.* **221**, 163–198, (1921).

73. R. Thomson, C. Hsieh, and V. Rana, Lattice trapping of fracture cracks, *J. Appl. Phys.* **42**(8), 3154–3160, (1971).

74. F. Rösch, C. Rudhart, J. Roth, H.-R. Trebin, and P. Gumbsch, Dynamic fracture of icosahedral model quasicrystals: A molecular dynamics study, *Phys. Rev. B.* **72**, 014128, (2005).

75. F. Rösch, H.-R. Trebin, and P. Gumbsch, Fracture of complex metallic alloys: An atomistic study of model systems, *Phil. Mag.* **86**(6–8), 1015–1020, (2006).

76. F. Rösch, H.-R. Trebin, and P. Gumbsch, Interatomic potentials and the simulation of fracture: C15 $NbCr_2$, *Int. J. Fracture.* **139**(3–4), 517–526, (2006).

77. J. B. Friauf, The crystal structure of Magnesium Di-Zincide, *Phys. Rev.* **29**(1), 34–40, (1927).

78. J. B. Friauf, The crystal structures of two intermetallic compounds, *J. Am. Chem. Soc.* **49**(12), 3107–3114, (1927).

79. F. Laves and H. Witte, Die Kristallstruktur des $MgNi_2$ und seine Beziehungen zu den Typen $MgCu_2$ und $MgZn_2$, *Metallwirtsch.* **14**(33), 645–649, (1935).

80. F. Laves and H. Witte, Der Einfluß von Valenzelektronen auf die Kristallstruktur ternärer Magnesiumlegierungen, *Metallwirtsch.* **15**(36), 840–842, (1936).

81. J. H. Wernick, *Topologically Close-Packed Structures*, In ed. J. H. Westbrook, *Intermetallic Compounds*, pp. 197–216. Wiley Series on the Science and Technology of Materials. John Wiley & Sons, Incorporated, (1967).

82. J. D. Livingston, Laves-phase superalloys?, *Phys. Stat. Sol. A.* **131**, 415–423, (1992).

83. P. M. Hazzledine and P. Pirouz, Synchroshear transformations in laves phases, *Scr. Mat. Metall.* **28**(10), 1277–1282, (1993).

84. P. Gumbsch, S. J. Zhou, and B. L. Holian, Molecular dynamics investigation of dynamic crack stability, *Phys. Rev. B.* **55**(6), 3445–3455, (1997).

85. J. Q. Guo, E. Abe, and A. P. Tsai, Stable icosahedral quasicrystals in binary Cd-Ca and Cd-Yb systems, *Phys. Rev. B.* **62**, R14605, (2000).

86. A. P. Tsai, J. Q. Guo, E. Abe, H. Takakura, and T. J. Sato, A stable binary

38   *H.-R. Trebin et al.*

quasicrystal, *Nature.* **408**, 537–538, (2000).

87. M. Widom and M. Mihalkovič, Order-disorder transition in the Cd-Ca cubic approximant, *Mat. Res. Soc. Symp. Proc.* **805**, LL1.10.1 LL1.10.6, (2004).

88. M. Mihalkovič and M. Widom, Canonical cell model of Cadmium-based icosahedral alloys, *Phil. Mag.* **86**(3–5), 519, (2006).

89. C. P. Gómez and S. Lidin, Comparative structural study of the disordered MCd_6 quasicrystal approximants, *Phys. Rev. B.* **68**, 024203, (2003).

90. R. Tamura, K. Edagawa, C. Aoki, S. Takeuchi, and K. Suzuki, Low-temperature structural phase transition in a Cd_6Y 1/1 approximant, *Phys. Rev. B.* **68**, 174105, (2003).

91. R. Tamura, K. Edagawa, Y. Murao, S. Takeuchi, K. Suzuki, M. Ichihara, M. Isobe, and Y. Ueda, Order-disorder transition in cubic Cd_6Yb and Cd_6Ca, *J. Non-Cryst. Solids.* **334&335**, 173–176, (2004).

92. K. Nozawa and Y. Ishii, First-principles studies on orientational ordering of atomic clusters in Cd_6Ca, *Phil. Mag.* **86**, 615–620, (2006).

93. P. Brommer, F. Gähler, and M. Mihalkovič, Ordering and correlation of cluster orientations in $CaCd_6$, *Accepted by Phil. Mag.* (2007).